# Statistical Analysis of Mesovortices During The First Rainy Season In South China

Ying Tang ( ✉ mg1628011@smail.nju.edu.cn )

Meteorological Bureau of Shenzhen Municipality

**Xin Xu**

Nanjing University

**Yuanzhao Chen**

Meteorological Bureau of Shenzhen Municipality

**Xunlai Chen**

Meteorological Bureau of Shenzhen Municipality

**Jiahao Liang**

Guangzhou Institute of Tropical and Marine Meteorology

**Jia Liu**

Meteorological Bureau of Shenzhen Municipality

**Yuan Wang**

Nanjing University

---

**Research Article**

# Abstract

Based on the Doppler radar observation and reanalysis data, the statistical characteristics of mesovortices (MVs) during the first rainy season (April–June) in South China from 2017 to 2019 are studied, including their spatio-temporal distributions, structural features and favorable environmental conditions. The results show that the MVs usually exhibit short lifetime, among which about 70% last for less than 30 minutes. The intensity and horizontal scale of the MVs are proportional to their lifetime. Long-lived MVs have larger horizontal scales and stronger intensities than short-lived ones. The MVs are mainly observed over the Pearl River Delta region, followed by the western Guangdong province, but relatively fewer in both eastern and northern Guangdong province. The uneven spatial distribution of the MVs is closely related to the differences of environment conditions over South China. The monsoonal south-westerlies, water vapor flux, atmospheric instability and vertical wind shear over southwest Guangdong are significantly larger than those in other regions, which are favorable for the formation of MVs. The occurrence frequencies of MVs in central and southern parts of Guangdong display similar diurnal variations, reaching the peak during the late afternoon and early evening, while dropping to the minimum overnight. However, the situation is opposite in northern Guangdong, with the peak overnight and the minimum during the late afternoon and early evening.

# Introduction

South China is an area with high frequency of severe convective weather, where disastrous weather such as short-term heavy rainfall, hail, tornado and gale frequently occur (Fan and Yu, 2013; Xue et al., 2019). Severe convective weather often causes serious casualties and property losses. For example, on April 13, 2016, a strong squall line process caused gusts in most of Guangdong Province, with the wind speed in most areas reaching 13.9 m·s$^{-1}$ (even up to 41.5–46.1 m·s$^{-1}$ in some areas). Meanwhile, it was also accompanied by short-term heavy rainfall, causing great economic losses (Wang et al., 2021). On March 4, 2018, a rarely-seen strong squall line occurred over the northern and central parts of Jiangxi Province. During this process, high wind speeds exceeding 17.2 m·s$^{-1}$ were found at 521 observational stations, among which the wind speeds at 172 stations were above 24.5 m·s$^{-1}$. This severe squall line affected more than 267,000 people and caused great damages to a large number of houses and crops, resulting in a direct economic loss of 410 million yuan (Zhang et al., 2019 ).

The forecasting of severe convective weather is one of the key challenging tasks in current weather forecast operation due to its small horizontal scale and the feature of abruptness (Yu et al., 2012). Studies have revealed that the severe convective weather is closely related to mesoscale convective systems (MCSs). However, previous studies mainly focused on the relationship between convective systems of meso-β-scale (with the horizontal scales ranging from 20 to 200 km, such as squall lines and bow echoes) and the strong convective weather (Evans and Doswell, 2001; Cohen et al., 2012). Slow-moving or quasi-stationary MCSs generally produce rainstorms (Schumacher and Johnson, 2005, 2006; Li et al., 2020), while fast-moving MCSs are prone to cause severe convective weather, such as short-time gales and tornadoes (Atkins et al., 2005; Funk et al., 1999). Du et al. (2020) investigated the effects of

topography, coastline and cold pool on convection development over the coastal regions of South China through a series of sensitivity experiments. It is found that the direction of cold pool outflow changes due to the terrain-blocking effects in coastal regions of South China, thereby affecting the development and movement of MCSs. Based on the Doppler radar data, Liu et al. (2018) analyzed an extreme precipitation event caused by two MCSs over the coastal regions of South China on May 11, 2014. It is suggested that the rapid splitting and reconstructing of the bow echoes in MCSs are more conducive to the occurrence of extreme precipitation. By using an objective identification algorithm for convection initiation based on radar mosaics, Bai et al. (2020) conducted a statistical study on the climatological characteristics of convections over the coastal regions of South China. Their results revealed that convection initiation exhibits three peaks, namely, a late-night-to-morning peak at windward coasts and offshore, a noon-to-late-afternoon peak on the coastal land, and an evening-to-early-morning peak over the northwestern highland.

With the progress of meteorological observation technology, especially the widespread application of Doppler weather radar and the continuous development of numerical models, increasing attention has been paid to the meso-γ-scale (with the horizontal scales being 2−20 km) or even smaller-scale convective systems. Several studies in recent years revealed that strong convective weather, such as tornadoes and severe straight-line winds, is directly caused by meso-γ-scale vortices within MCSs (Trapp et al., 2003; Xu et al., 2015). By using the Advanced Research Weather Research and Forecasting model, Atkins and Laurent (Atkins and Laurent, 2009) investigated the relationship between the vertical wind shear and disastrous gales. It is indicated that strong low-level wind shear can cause strong vortices in the bow echo, while the consistency in directions of the descending rear inflow jet and the meso-γ-scale vortices leads to surface gales. Similarly, Funk et al. (1999) detailedly analyzed a storm that occurred over Kentucky and northern Indiana on April 15, 1994. Their results show that the occurrence of disastrous gales is closely related to the meso-γ-scale vortices generated at the apex of the bow echoes in the lower level. Long-lived and deep meso-γ-scale vortices can develop into tornadoes and result in widespread disastrous gales. By analyzing the proportion of tornadic mesocyclones based on Doppler radar observations, Trapp et al. (2005) suggested that about 26% meso-γ-scale vortices can develop into tornadoes.

Meso-γ-scale vortices can be classified into two types. One is mesocyclones caused by convective storm cells (Burgess et al., 1993), and the other is the so-called mesovortices (MVs) generated in the low level of organized MCSs (Funk et al. 1999). In the past, domestic studies on meso-γ-scale vortices mainly focused on mesocyclones (Yu et al., 2006; Feng et al., 2010; Fang and Zheng, 2007). Taking the case of a thunderstorm gale for example, a squall line appeared during the convection's southeastward-moving process from the west of Hunan to Guangdong on March 20, 2013 (Fang et al., 2015). There are many supercells within this squall line, and most of the thunderstorm gales are generated from the mesocyclones of the supercells. Nonetheless, there is a lack of thorough studies on MVs in China. Recently, Tang et al. (2020, hereafter T20) carried out a statistical analysis of MVs during the warm season in the Yangtze-Huaihe River Basin (YHRB). Their results showed that most of the MVs in this region have a short lifetime, with an average of 26 minutes. Long-lived MVs generally have larger size

than those of short-lived MVs. However, there are few studies on the MVs in other regions of China, such as South China.

In this paper, we statistically analyze the MVs in the first rainy season in South China during 2017–2019 according to Doppler radar observations. Combined with the reanalysis data, we further study the environmental characteristics of the MVs to find out their favorable conditions. Furthermore, the MVs in South China are compared to those in the YHRB. The remainder of this paper is organized as follows. Data and methods are introduced in Sect. 2. The main results are presented in Sect. 3. Finally, the conclusions and discussions are provided in Sect. 4.

# Data And Methods

## 2.1 Data

In this paper, observations from nine Doppler weather radars in Guangdong from April to June in 2017–2019 are used. The distribution of these radar stations is shown in Fig. 1, covering almost the whole Guangdong Province. As in T20, the 88D2ARPS program of the Advanced Regional Prediction System (ARPS) from the Center for Analysis and Prediction of Storms (CAPS) at the University of Oklahoma (Xue et al., 2000) is used for the raw radar data quality control, which removes non-meteorological echoes and performs the radial velocity dealiasing (Brewster et al., 2005). The processed radar data is further used to identify and statistically analyze the MVs. Finally, the ERA5 reanalysis data (Hersbach and Dee, 2016) with a high horizontal resolution of 0.25° × 0.25° from the European Centre for Medium-Range Weather Forecasts (ECMWF) is utilized to study the environmental conditions for MVs in Guangdong from April to June.

## 2.2 Identification of MVs

Since MVs are mainly generated in organized MCSs, it is necessary to identify the MCSs in advance. Firstly, the composite reflectivity from the nine Doppler radars (Figure 1) is used to identify convective zones (CZs) of >35 dBZ. Then, the area of each CZ is calculated, and the CZ with an area greater than 1000 km$^2$ is considered as a MCS. More details about the detection of MCSs can be found in T20.

In the past, the identification of meso--scale vortices (e.g., mesocyclones) or even smaller-scale circulations (e.g., tornadoes) mainly depends on the appearance of positive-negative velocity pair in the Doppler radar radial velocity field (Mitchell et al., 1998). The rotational strength of a vortex is measured by the difference between the maximum inbound and outbound radial velocities which is, however, susceptible to the velocity noises. When the environmental wind speed is strong, the positive-negative velocity cannot be identified because it is easily submerged in the background wind field. Moreover, when the vortex is far from the radar station, the azimuthal resolution becomes too low to well resolve the velocity pair. In this paper, a more advanced linear least square derivative method (Smith and Elmore, 2004) is used to calculate the azimuthal shear of the MV. This method synthetically considers the

contribution of all radial velocities in a given range to the azimuthal shear at the center point, thus reducing the noise errors caused by the radial velocities.

In this study, we only calculate the azimuthal shear at the 0.5° elevation within 150 km of the radar because the MVs are mainly generated in the lower troposphere below 3 km. As in T20, a lower limit of $10^{-3}$ s$^{-1}$ is adopted for the azimuthal shear of MVs, which is one order greater than the Coriolis parameter in mid latitudes. The duration of the MV must exceed 18 minutes, i.e., three volume scans of the radar. On this basis, a storm cell identification technology similar to WSR-88D is adopted for the forward and backward tracking of MVs to obtain their life cycles (Johnson et al., 1998).

Because the radar radial velocity cannot be composed, the identification of MVs can only be performed for each individual radar. Despite the dense distribution of Doppler radars in Guangdong Province, only four radars covering almost the whole province are selected to identify the MVs. These four radars include Shaoguan (9751), Shantou (9754), Yangjiang (9662) and Guangzhou (9200) radar stations, representing the northern, eastern, western Guangdong Province and the Pearl River Delta region, respectively.

# Characteristics Of Mvs During The First Rainy Season In South China

### 3.1 Spatio-temporal distribution

During the first rainy season (April–June) in South China from 2017 to 2019, a total of 7,965 MVs are identified using the four radars in Guangdong Province (Table 1). Figure 2 shows the uneven spatial distribution of MVs in Guangdong Province. The MVs are most concentrated in the Pearl River Delta region (Figure 2a), accounting for about 41% of the total, followed by the western Guangdong (Figure 2b) where the MVs account for about 27%. There are much fewer MVs generated in eastern (Figure 2d) and northern Guangdong (Figure 2c), which together account for less than half of the total. In particular, the MVs are sparsely distributed near the Nanling mountains in northern Guangdong. The uneven spatial distribution of the MVs can be, at least, attributed to the following two reasons. The first is due to the different topographies features over Guangdong. Laing and Fritsch (1997) have pointed out that MVs are prone to form over flat regions, such as the America Great Plains. The formation of MVs is therefore affected by the topography of the Nanling mountains in northern Guangdong and the Lianhua, Luofu and Jiulian Mountains in eastern Guangdong. In contrast, the relatively flat terrain in western Guangdong and Pearl River Delta region is conducive to the formation of the MVs. Secondly, the uneven spatial distribution of MVs is intimately related to the differences of environmental conditions in different regions of Guangdong, which will be discussed in section 3.3. In terms of lifetime, most of the MVs (about 67%) last less than 30 minutes, about 30% last more than half an hour, while the ones lasting more than one hour only account for about 5% (Table 1). The statistical characteristics of MVs' lifetime in Guangdong are similar to those in the YHRB.

Table 1. Statistics for the number and lifetime of the MVs identified by four radars in Guangdong from April to June during 2017−2019. Percentages of the MVs with different lifetime to the total are shown in parentheses.

|  | Guangzhou | Shaoguan | Yangjiang | Shantou | Total |
|---|---|---|---|---|---|
| Number of MVs | 3267 | 794 | 2182 | 1722 | 7965 |
| 18−30 min | 2153 (66%) | 551 (69%) | 1466 (67%) | 1172 (68%) | 5342 (67%) |
| 30−60 min | 992 (30%) | 223 (28%) | 626 (29%) | 479 (28%) | 2320 (29%) |
| >60 min | 122 (4%) | 20 (3%) | 90 (4%) | 71 (4%) | 303 (4%) |

Figure 3 shows the monthly and daily variations of the MVs in South China. The number of MVs generated in June is significantly larger than in April and May, accounting for about half of the total (Figure 3a). Besides, the MVs display notable diurnal variations (Figure 3b). It occurs most frequently from the late morning to the afternoon (0900 BJT to 1800 BJT, i.e., Beijing time) but drops to the minimum overnight (2100 BJT to 0300 BJT). This diurnal variation is just opposite to that in the warm season in the YHRB (Tang et al., 2020). Specifically, the MVs in the YHRB present slight diurnal variations (figures omitted), with two weak peaks at night (1800 BJT to 2100 BJT) and in the morning (0600 BJT to 0900 BJT), respectively. Besides, there is a minimum at night (0300 BJT to 0600 BJT).

Figure 4 shows the distributions of the diameters and intensities (in terms of azimuthal shear) of the MVs. It can be seen that the MV diameters are mostly between 4 km and 12 km (about 80%), while only a few ones are larger than 12 km or smaller than 4 km (Figure 4a). Most of the MVs (about 94%) are weak, with the intensities between 0.001 $s^{-1}$ and 0.004 $s^{-1}$, while only about 6% are stronger than 0.004 $s^{-1}$ (Figure 4b). It is indicated that the diameter of the MV is proportional to its lifetime (Table 2). The MVs presenting a short lifetime of 18−30 minutes have a mean diameter of 6.96 km, the MVs lasting for 30−60 minutes have a mean diameter of 8.35 km, and the MVs lasting for more than one hour have a mean diameter of 10.3 km. Similarly, the azimuthal shear of the MVs is also proportional to their lifetime. The MVs with a short lifetime of 18−30 minutes have an average intensity of 0.002 $s^{-1}$, while the MVs with a long lifetime of exceeding 60 minutes have an average intensity of 0.003 $s^{-1}$. Thus, a longer lifetime is accompanied with greater diameter and stronger intensity, which is similar to the characteristics of the MVs in the YHRB.

Table 2. Average diameter, azimuthal shear intensity and lifetime of the MVs in Guangdong from April to June during 2017−2019.

|  | Diameter (km) | Azimuthal shear ($0^{-3} \cdot s^{-1}$) | Lifetime (minutes) |
|---|---|---|---|
| All MVs | 7.49 | 2.15 | 26 |
| Short-lived MVs | 6.96 | 2.03 | 20 |
| Medium-lived MVs | 8.35 | 2.33 | 36 |
| Long-lived MVs | 10.30 | 2.88 | 75 |

### 3.2 Comparison of MVs in different regions of South China

As mentioned above, most MVs during the first rainy season in Guangdong appear in the Pearl River Delta region and western Guangdong. In this subsection, the temporal variations of MVs in different regions of South China are compared. About half of the MVs in the Pearl River Delta region occur in June, which is significantly more than that in April and May (not shown). Similar monthly variations of MVs are found in eastern Guangdong. However, there are no significant monthly variations in northern and western Guangdong. The number of MVs generated in each month (April to June) is almost the same Figure 5(a).

The diurnal variations are quite similar for the MVs in the River Delta region, western and eastern Guangdong (Figure 5), which show an afternoon-to-night peak and night-to-early-morning minimum. However, the MVs in northern Guangdong present an opposite diurnal variation, along with a night-to-early-morning peak and afternoon-to-evening minimum. This may be explained by the moving direction of MCSs in Guangdong. During the first rainy season in South China, there is still weak cold air frequently affecting Guangdong from the north. Under the combined influence of dry and cold air from the north and warm and moist air from the sea, there is usually an MCS accompanied by a cold front, affecting Guangdong from the north to the south. The MCS tends to be triggered in northern Guangdong during the night-to-morning period, and then moves eastward and southward to southern Guangdong from the afternoon to evening (Wu et al., 2019). Therefore, the MVs generated in the MCS present consistent diurnal variations with that of the MCSs.

Moreover, the statistical characteristics of the MVs' lifetime in the Pearl River Delta region is similar to that in other three regions, with the average lifetime of 25-30 minites. The azimuthal shear intensity and horizontal scale of the MVs are also similar in the Pearl River Delta region and northwest Guangdong, with the average diameter of about 7 km and the average intensity of about 0.002 $s^{-1}$. The MVs in eastern Guangdong are slightly weaker and smaller than the other three regions. (Table 3).

Table 3. Average diameter, azimuthal shear intensity and lifetime of the MVs in different regions of Guangdong from April to June during 2017−2019.

| | Diameter (km) | Azimuthal shear ($0^{-3} \cdot s^{-1}$) | Lifetime (minutes) |
|---|---|---|---|
| the Pearl River Delta | 7.64 | 2.16 | 27 |
| Western Guangdong | 7.54 | 2.23 | 26 |
| Northern Guangdong | 7.34 | 2.28 | 25 |
| Eastern Guangdong | 7.22 | 1.98 | 26 |

### 3.3 Environmental conditions

As noted above, the spatial distribution of the MVs during the first rainy season in South China is affected by their environmental conditions. During this period, the South Asia high center is located in the upper troposphere (200 hPa) over the Indochina Peninsula and adjacent areas (Figure 6a). South China is on the southern side of the upper-level jet axis at its entrance region. In the middle troposphere (500 hPa), the subtropical high lies between 10°N and 20°N, and South China lies on the northern side of the subtropical high and in the westerlies at the bottom of the East Asia trough (Figure 6b). In the lower troposphere (850 hPa), with the onset of the southwest monsoon, the equatorial westerlies from the Indian Ocean and the cross-equatorial flow from near Kalimantan Island entering the South China Sea converge and blow over South China (Figs. 6c and 6d). Meanwhile, the low-level southwesterly jets transport abundant warm and moist air to South China, especially to the west of the Pearl River Estuary (the Pearl River Delta region and western Guangdong), resulting in the higher potential pseudo-equivalent temperature and water vapor flux in this region than in northern and eastern Guangdong.

Due to the warm and moist airflow transported by the southwest monsoon, the mean low-level instability during April–June is relatively higher across the whole Guangdong Province (Figure 7a). The potential pseudo-equivalent temperature in southwest Guangdong (30°C–32°C) is significantly higher than that in other regions (28°C–30°C). In addition, the existence of the low-level jet causes stronger low-level wind shear over southwest Guangdong than in other regions (Figure 7b). In short, the relatively higher instability and stronger low-level vertical wind shear are conducive to the formation of MVs, which is similar to the environmental conditions for the formation of MVs in the YHRB. Weisman and Trapp (2003) simulated the effects of vertical wind shear on the genesis of MVs. The results show that the stronger the vertical wind shear is, especially for the low-level wind shear, the stronger the MVs will be. Atkins and Laurent (2009) obtained a similar result by using the Advanced Research Weather Research and Forecasting model to study the relationship between the MVs and the low-level wind shear.

## Conclusions And Discussion

In this paper, the mesovortices (MVs) occurred during the first rainy season (April to June) in South China during 2017–2019 are analyzed using Doppler radar observations as well as ERA5 reanalysis. The spatio-temporal distributions and structural features of MVs are examined, as well as their favorable environmental conditions. The main conclusions are as follows.

The MVs are mainly observed in the Pearl River Delta region, followed by western Guangdong, and relatively fewer in both eastern and northern Guangdong. Similar to the Yangtze-Huaihe River Basin (YHRB), the MVs in South China present very short lifetime, with about 70% lasting less than 30 minutes. The intensity and horizontal scale of the MVs are proportional to their lifetime, i.e., long-lived MVs have larger horizontal scales and stronger intensities than short-lived ones. Different from the MVs in the YHRB, the MVs in South China display more significant diurnal variations, which occur most frequently from late morning toward evening (1100 BJT to 1700 BJT) but drop to the minimum overnight (2000 BJT to 0200 BJT on the next day). In contrast, the MVs in the YRHB present slight diurnal variations, with two weak peaks at night (1800 BJT to 2100 BJT) and in the morning (0600 BJC to 0900 BJT) as well as a minimum in the early morning (0300 BJT to 0600 BJT).

The diurnal variations are quite similar for the MVs in the Pearl River Delta region, western and eastern Guangdong, with an afternoon-to-evening peak and a night-to-early-morning minimum. On the contrary, the diurnal variation of MVs in northern Guangdong is opposite to that mentioned above. This is because during the first rainy season in South China, under the combined influence of dry and cold air from the north and the warm and moist air from the sea, there is usually an MCS accompanied by a cold front, which thereby affects South China from north to south. The MCS tends to be triggered in northern Guangdong from night to morning, and then moves to the southern coastal areas from afternoon to evening. As a result, MVs generated within MCSs have a similar diurnal variations to their parent systems.

The uneven spatial distribution of MVs is closely related to the environmental differences in South China. Affected by the southwest monsoon, the water vapor flux, low-level instability and vertical wind shear in southwest Guangdong are significantly greater than those in other regions during the first rainy season, which are favorable to the formation of MVs.

This study contributes to the understanding of MVs in South China and thus has a great significance for the operational nowcasting and warning of MVs. However, the relationship between the MVs and severe weather (such as gales, heavy rainfall) in South China is still unclear, which will be studied in the future.

# Declarations

**Conflicts of Interest** *The authors declare no conflict of interest.*

**Availability of data and material** *The data that support the findings of this study are available from the first author, upon reasonable request.*

**Code availability** *The codes that support the findings of this study are available from the first author.*

**Ethics approval** *The authors declare that there is no human or animal participant in the study. Not applicable.*

**Consent to participate** *The authors declare that there is no human or animal participant in the study. Not applicable.*

**Consent for publication** *The authors give their consent to the publication of all details of the manuscript including texts, figures, and tables.*

# References

1. Atkins NT, Bouchard CS, Przybylinski RW, Trapp RJ, Schmocker G (2005) Damaging surface wind mechanism within the 10 June 2003 Saint Louis bow echo during BAMEX. Mon Weather Rev 133:2275–2296

2. Atkins NT, Laurent MSt (2009) Bow echo mesovortices. Part I: Processes that influence their damaging potential. Mon Weather Rev 137:1497–1513

3. Bai L, Chen G, Huang L (2020) Image processing of radar mosaics for the climatology of convection initiation in South China[J]. Journal of Applied Meteorology Climatology 59(1):65–81

4. Brewster K, Hu M, Xue M, Gao J (2005) Efficient assimilation of radar data at high resolution for short-range numerical weather prediction. World Weather Research Program Symposium on Nowcasting & Very Short-range Forecasting 2008. [Available online at http://twister.ou.edu/papers/BrewsterWWRP_Nowcasting.pdf.]

5. Burgess DW, Donaldson RJ Jr, Desrochers PR (1993) Tornado detection and warning by radar. The Tornado: Its structure, dynamics, prediction and hazards. Geophys. Monogr. No. 79, Amer. Geophys. Union, pp 203–221

6. Cohen AE, Coniglio MC, Corfidi SF, Corfidi SJ (2012) Discrimination of mesoscale convective system environments using sounding observations. Wea Forecasting 22(5):1045

7. Davis JM, Parker MD (2014) Radar climatology of tornadic and non-tornadic vortices in high-shear, low-CAPE environments in the mid-Atlantic and Southeastern United States. Wea Forecasting 29:828–853

8. Du Y, Chen G, Han B et al (2020) Convection initiation and growth at the coast of South China. Part II: effects of the terrain, coastline and cold pools[J]. Mon. Weather Rev. 148(9)

9. Evans JS, Doswell CA (2001) Examination of derecho environments using proximity soundings. Wea Forecasting 16(3):329–342

10. Fan L, Yu X (2013) Characteristic analyses on environmental parameters in short-term severe convective weather in China. Plateau Meteorology 32(1):156–165

11. Fang C, Yu X, Zhu W et al (2015) Characteristics of the thunderstorm gale process in Hunan and Guangdong on 20 March 2013. Meteorological Monthly 41(11):1305–1314

12. Fang C, Zheng Y (2007) The analysis of mesocyclone product from the Doppler weather radar. Meteorological Monthly 33(11):18–22

13. Feng J, Tang D, Yu X et al (2010) The accuracy statistics of mesocyclone identification products from CINRAD/SA. Meteorological Monthly 36(8):47–52

14. Funk TW, Darmofal KE, Kirkpatrick JD, Dewald VL, Przybylinski RW, Schmocker GK, Lin Y-J (1999) Storm reflectivity and mesocyclone evolution associated with the 15 April 1994 squall line over Kentucky and southern Indiana. Wea Forecasting 14:976–993

15. Hersbach H, Dee D (2021) ERA5 reanalysis is in production. ECMWF Newsletter 147:7–7. https://www.ecmwf.int/en/newsletter/147/news/era5-reanalysis-production Available online at

16. Johnson JT, Mackeen PL, Witt A, Mitchell ED, Stumpf GJ, Eilts MD et al (1998) The storm cell identification and tracking algorithm: An enhanced WSR-88D algorithm. Wea Forecasting 13:263–276

17. Li H, Wan Q, Peng D et al (2020) Multiscale analysis of a record-breaking heavy rainfall event in Guangdong, China[J]. Atmos. Res. 232(Feb.), 104703.1-104703.13

18. Laing AG, Fritsch JM (1997) The global population of mesoscale convective complexes. Quart J Roy Meteor Soc 123:389–405

19. Liu X, Luo Y, Guan Z et al (2018) An extreme rainfall event in coastal South China during SCMREX-2014: Formation and roles of rainband and echo trainings[J]. Journal of Geophysical Research, Atmospheres, 123

20. Mitchell ED, Vasiloff SV, Stumpf GJ, Witt A, Eilts MD, Johonson JT, Thomas KW (1998) The national severe storms laboratory tornado detection algorithm. Wea Forecasting 13:352–366

21. Schumacher RS, Johnson RH (2005) Organization and environmental properties of extreme-rain-producing mesoscale convective systems. Mon Weather Rev 133(4):961–976

22. Schumacher RS, Johnson RH (2006) Characteristics of U.S. extreme rain events during 1999–2003. Wea Forecasting 21:69–85

23. Smith TM, Elmore KL (2004) The use of radial velocity derivatives to diagnose rotation and divergence. 11th Conf. on Aviation, Range, and Aerospace, Hyannis, MA, Amer. Meteor. Soc., P5.6. [Available online at http://ams.confex.com/ams/pdfpapers/81827.pdf.]

24. Tang Y, Xu X, Xue M et al (2020) Characteristics of low-level meso-γ-scale vortices in the warm season over East China[J]. Atmos. Res. 235

25. Trapp RJ, Tessendorf SA, Godfrey ES, Brooks HE (2005) Tornadoes from squall lines and bow echoes. Part I: climatological distribution. Wea Forecasting 20(1):23–34

26. Trapp RJ, Weisman ML et al (2003) Low-Level mesovortices within squall lines and bow echoes. Part II: Their genesis and implications.[J]. Mon. Weather Rev

27. Wang L, Shen X, Wang Y et al (2021) Mechanism analysis of a squall line upscale growing process in South China [J]. Plateau Meteorology 40(1):145–158

28. Weisman ML, Trapp RJ (2003) Low-Level mesovortices within squall lines and bow echoes. Part I: Overview and dependence on environmental shear[J]. Mon Weather Rev 131(11):2779–2803

29. Wu N, Ding X, Wen Z et al (2019) Contrasting frontal and warm-sector heavy rainfalls over South China during the early-summer rainy season[J]. Atmospheric Research, p 235

30. Xu X, Xue M, Wang Y (2015) The genesis of mesovortices within a real data simulation of a bow echo system. J. Atmos. Sci. 72(5).

31. Xue M, Droegemeier KK, Wong V (2000) The Advanced Regional Prediction System (ARPS)—A multi-scale nonhydrostatic atmospheric simulation and prediction model. Part I: Model dynamics and verification. Meteor Atmos Phys 75:161–193

32. Xue X, Ren G, Sun X et al (2019) Climatological characteristics of meso-scale and micro-scale strong convective weather events in China [J]. Climatic Environmental Research (in Chinese) 24(2):199–213

33. Yu X, Zheng Y, Zhang A et al (2006) The detection of a severe tornado event in Anhui with China new generation weather radar. Plateau Meteorology 25(5):914–924

34. Yu X, Zhou X, Wang X (2012) The advances in the nowcasting techniques on thunderstorms and severe convection. Acta Mereorologica Sinica 70(3):311–337

35. Zhang C, Zhi S, Xu A (2019) Analysis of radar echo characteristics of rare force 10 gale with a strong squall line event in Jiangxi [J]. Torrential Rain Disasters 38(2):135–143
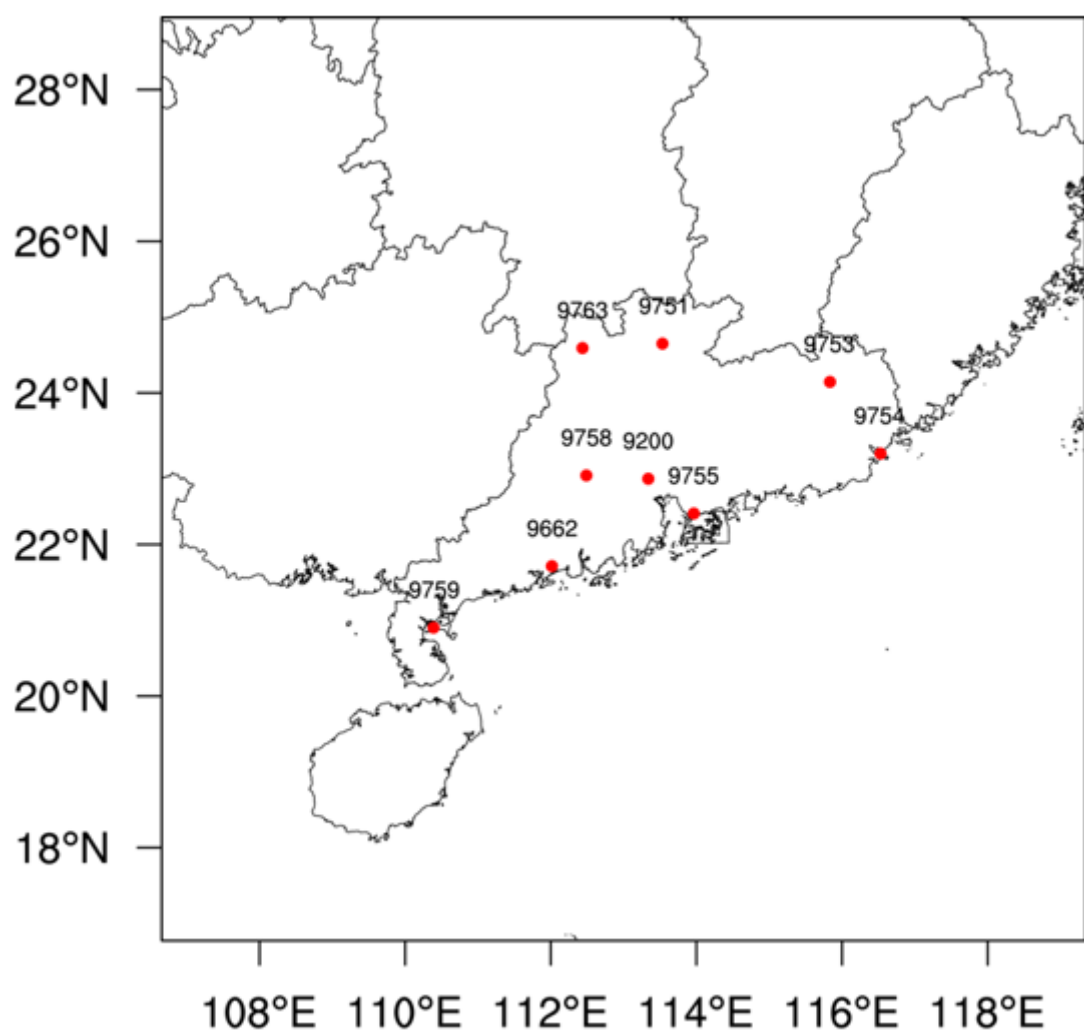
# Figures

**Figure 1**

Distribution of nine Doppler weather radars (red dots) in Guangdong, including Guangzhou (9200), Yangjiang (9662), Shaoguan (9751), Meizhou (9753), Shantou (9754), Shenzhen (9755), Zhaoqing (9758), Zhanjiang (9759) and Lianzhou (9763) radar stations. Note: The designations employed and the presentation of the material on this map do not imply the expression of any opinion whatsoever on the part of Research Square concerning the legal status of any country, territory, city or area or of its authorities, or concerning the delimitation of its frontiers or boundaries. This map has been provided by the authors.
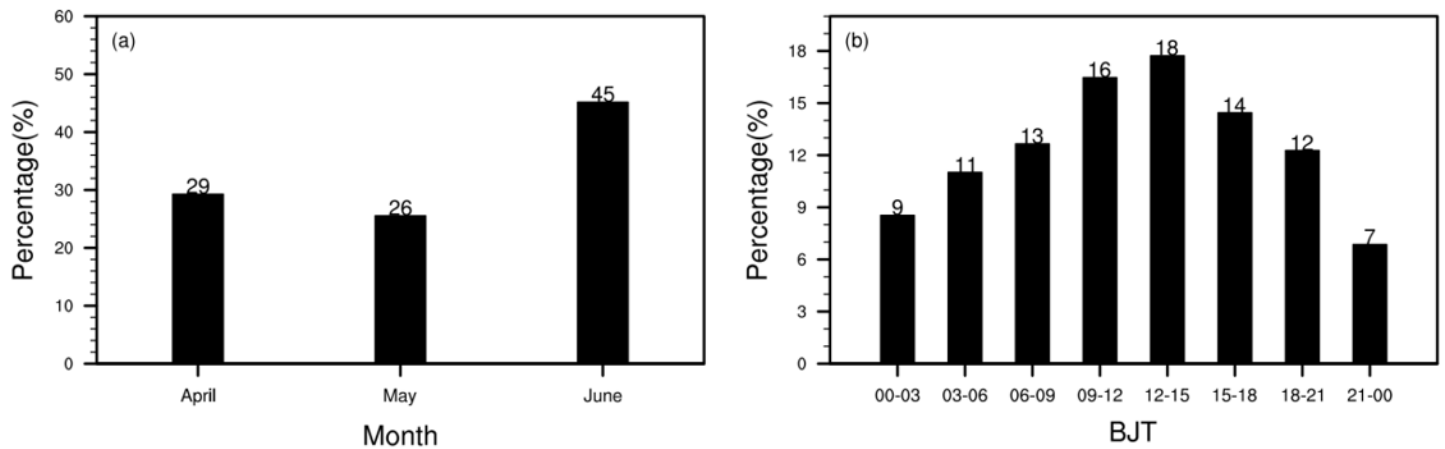
## Figure 2

Distributions of the MVs in (a) the Pearl River Delta region, (b) western Guangdong, (c) northern Guangdong and (d) eastern Guangdong during the first rainy season in South China from 2017 to 2019. Note: The designations employed and the presentation of the material on this map do not imply the expression of any opinion whatsoever on the part of Research Square concerning the legal status of any country, territory, city or area or of its authorities, or concerning the delimitation of its frontiers or boundaries. This map has been provided by the authors.

## Figure 3

(a) Monthly and (b) diurnal variations of the MVs in Guangdong from April to June during 2017−2019.
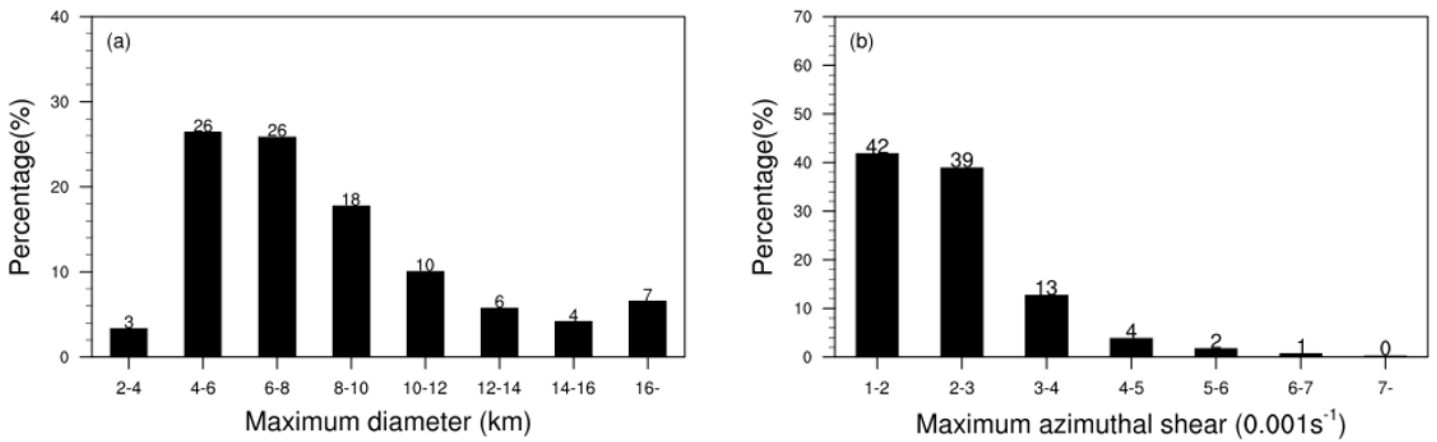


## Figure 4

Distributions of the (a) diameter (km) and (b) intensity (10−3•s−1) of the MVs in Guangdong from April to June during 2017−2019.
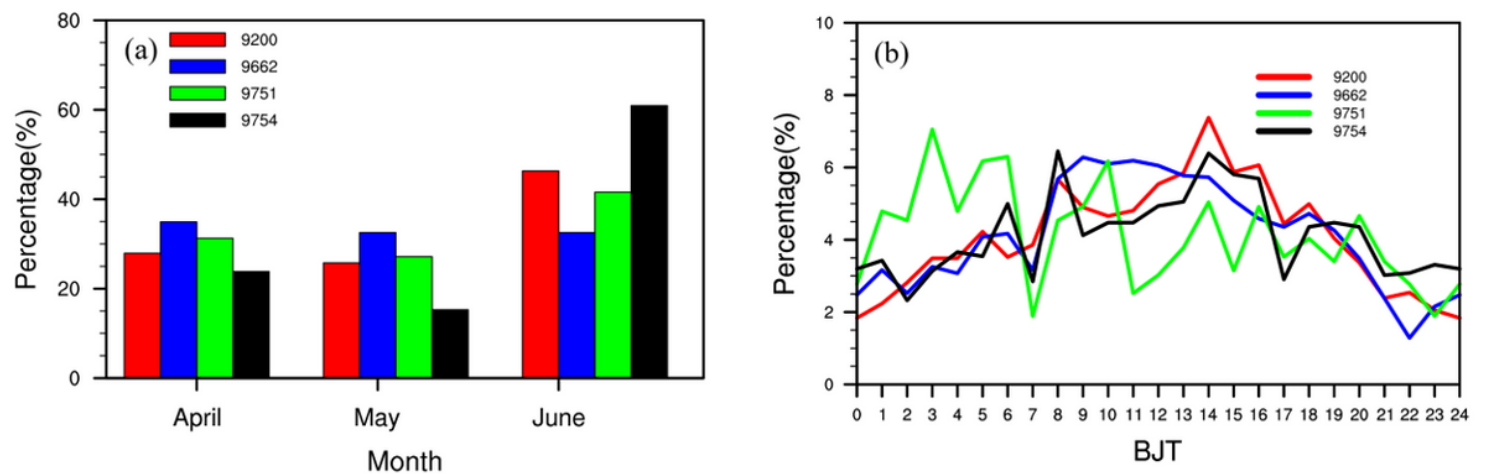
## Figure 5

(a) Monthly variations and (b) diurnal variations of MVs in the four different regions of Guangdong. Red bar (solid line) represents the Pearl River Delta region, blue bar (solid line) represents western Guangdong, green bar (solid line) represents northern Guangdong, and black bar (solid line) represent eastern Guangdong.
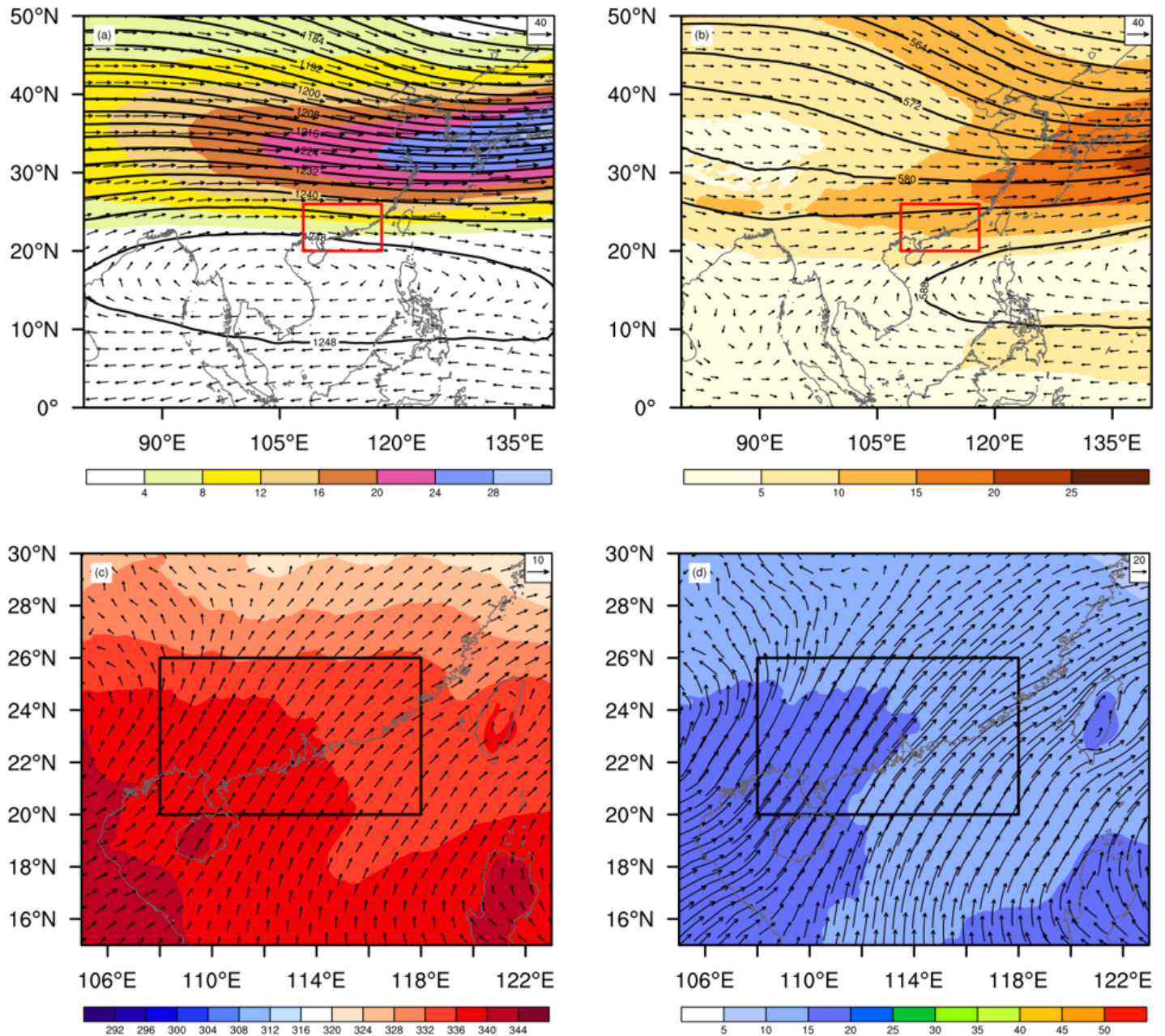


## Figure 6

Wind fields (arrows and shaded, unit: m•s−1) and geopotential height fields (black contours, unit: m) during April–June in (a) East Asia at 200 hPa and (b) Pan-South China at 500 hPa; (c) wind field (arrows, unit: m•s−1) and potential pseudo-equivalent temperature (shaded, unit: K) in Pan-South China at 850

hPa; (d) water vapor flux (arrows and shaded, unit: g•cm−1•hPa−1•s−1) in Pan-South China at 850 hPa. Both the red and black boxes represent Guangdong Province. Note: The designations employed and the presentation of the material on this map do not imply the expression of any opinion whatsoever on the part of Research Square concerning the legal status of any country, territory, city or area or of its authorities, or concerning the delimitation of its frontiers or boundaries. This map has been provided by the authors.
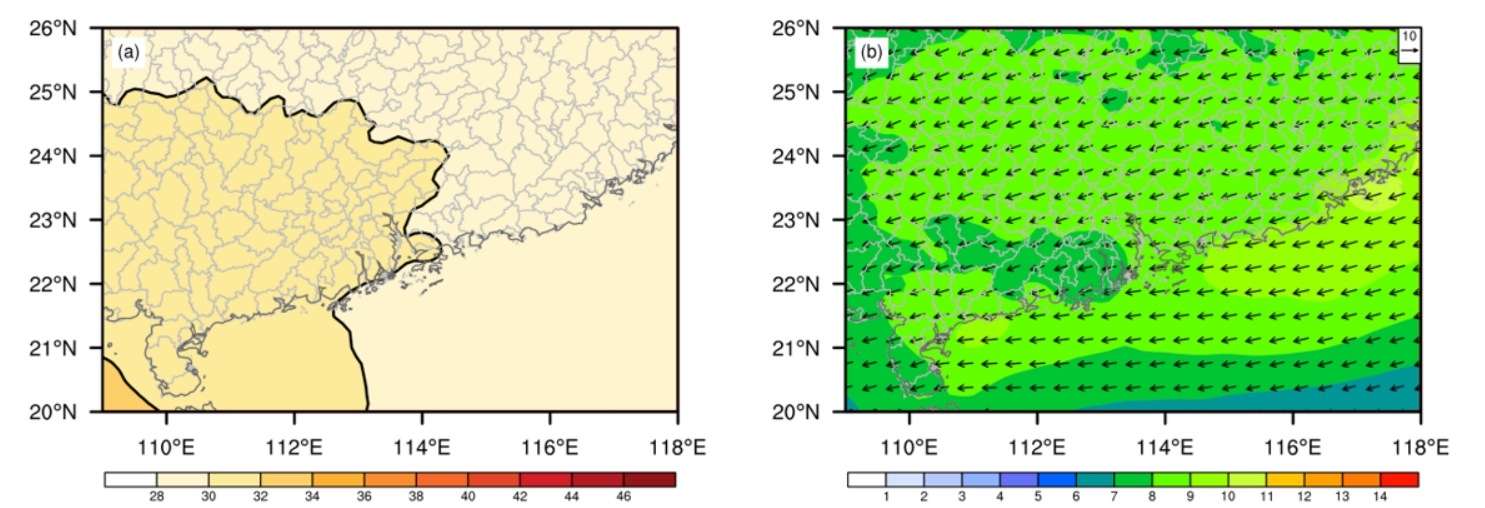


## Figure 7

(a) Potential pseudo-equivalent temperature (shaded and black contours, unit: °C) and (b) vertical wind shear (shaded and arrows, unit: m•s−1) at 1000−700 hPa in Guangdong from April to June. Note: The designations employed and the presentation of the material on this map do not imply the expression of any opinion whatsoever on the part of Research Square concerning the legal status of any country, territory, city or area or of its authorities, or concerning the delimitation of its frontiers or boundaries. This map has been provided by the authors.